Open Access
Original paper

Budownictwo i Architektura – Civil and Architectural Engineering 24(4) (2025) 25002
https://doi.org/10.35784/bud-arch.7250

The influence of layer interaction models and horizontal loads on flexible pavement strain responses

Andi Muflih Marsuq Muthaher[1*], Anno Mahfuda[2], Muh Bahrul Ulum Al Karimi[3]

[1] *Department of Civil Engineering and Planning; Vocational College; Universitas Diponegoro; 13 Prof. Soedarto St., Semarang, Indonesia, andimuflih@lecturer.undip.ac.id*
[2] *Department of Civil Engineering and Planning; Vocational College; Universitas Diponegoro; 13 Prof. Soedarto St., Semarang, Indonesia, annomahfuda@lecturer.undip.ac.id*
[3] *Department of Civil Engineering and Planning; Vocational College; Universitas Diponegoro; 13 Prof. Soedarto St., Semarang, Indonesia, mbualkarimi@lecturer.undip.ac.id*

[*] *Corresponding Author*
Received: 08.02.2025; Revised: 14.06.2025; Accepted: 20.10.2025; Available online:16.12.2025

Abstract:
This study investigates the influence of interlayer bonding conditions and horizontal loading on the mechanistic response of flexible pavements using Finite Element (FE) analysis. A spectrum of interface models – frictionless, simple friction, and full bond – was analyzed, and the resulting pavement strains were benchmarked against the perpetual pavement criteria established by the National Center for Asphalt Technology (NCAT). The results indicate that subgrade rutting is the dominant failure mode, with vertical compressive strains exceeding the 200 με NCAT threshold in most realistic bonded scenarios. A critical finding is the distinct impact of the analyzed parameters on different failure modes: horizontal loads were found to significantly increase tensile strains in the asphalt layer (fatigue risk) but had a negligible effect on compressive strains at the subgrade level (rutting risk). These findings highlight the necessity of including horizontal loads in fatigue analysis and demonstrate that the simple friction model provides a realistic intermediate condition between the idealized performance boundaries of the full bond and frictionless states. The study concludes by recommending further research to calibrate practical interface parameters to enhance the accuracy of pavement performance predictions.

Keywords:
flexible pavement strain responses, interlayer bonding conditions, horizontal loads, Finite Element (FE) analysis

1. Introduction

Flexible pavement comprises several layers: bituminous, granular (bound or unbound), and subgrade. The asphalt layer consists of bituminous material, while the granular layer is composed of high-quality geomaterials, specifically coarse-grained unbonded materials, and the subgrade consists of geotechnical materials. These layers are crucial for withstanding repeated traffic loads, particularly the asphalt layer, which is vital as it must be designed to be strong and highly durable to withstand stresses. Meanwhile, the base and subbase layers transfer these stresses to the subgrade layer [1,2]. The analysis and design of flexible pavements heavily rely on data obtained by measuring the pavement's response to the stress and strain distribution caused by tyre loads [3].

The multilayer linear elastic theory has long served as the foundation for analyzing the performance of road pavements, particularly in determining optimal layer thickness and predicting stress, strain, and deflection responses under traffic loads. Within this framework, mathematical models such as the Burmister and Boussinesq theories operate under the assumption of either no friction between the layers or perfect adhesion [4]. Two extreme conditions related to these interface conditions are full friction (full bond) and frictionless (full slip) [5]. KENLAYER has also been developed based on these extreme conditions [6].

Preliminary studies on friction between pavement layers have been conducted with case studies on flexible pavements and overlays on rigid pavements. The system's behaviour is analyzed using a linear frictional model with the parameter modulus of resistance to displacement, *K*, which can be determined from pure shear tests in the laboratory. The varying parameter *K* is used in flexible pavements between the asphalt-to-asphalt layer and the asphalt-to-base layer. *K* is assigned an infinite value to signify very rough friction. The study's findings reveal that when the interface condition shifts from rough (*K* value > 10,000 kg/cm³) to smooth (*K* value < 100 kg/cm³), there is a notable increase in vertical stress at the base of the surface layer [7].

Constitutive models for the interface of flexible pavements determine the mechanical property effects of that interface on the performance of road pavements. The modelling is conducted on the asphalt-asphalt layer through direct shear tests and fatigue tests, which show that applying tack coat on the interface between betwixt asphalt layers provides greater durability to that layer than when tack coat is not applied. Meanwhile, field tests on the asphalt-granular layer show that the asphalt layer can be seen as fully bonded to the granular layer because it resists movement well [8].

The BISAR program by Shell was developed to predict the behaviour of multilayer systems within the linear elastic framework. Besides modelling general parameters within the linear elastic concept, this program can also model the interface bonding conditions specified in each layer [9]. In modelling the interaction between layers, BISAR applies the concept and parameter of shear spring compliance, or AK, which can model slip between layers. The AK parameter is the inverse of the shear

reaction modulus, Ks, based on Goodman's constitutive law [10]. From several studies using BISAR, good adhesion between each pavement layer can reduce critical stress values, thereby improving the pavement's structural capacity as the adhesion or friction increases [5].

The horizontal load effect on flexible pavement is a critical factor influencing its structural integrity and longevity. Horizontal loads, typically generated by traffic wheels, can worsen pavement issues like slippage cracking, fatigue cracking, and delamination of the surface layer, mainly when the adhesion between asphalt layers is weak [11]. These loads contribute to increased horizontal tensile strain, a significant factor in fatigue cracking [12].

This study analyses the influence of asphalt layer interaction models on the strain response resulting from adding horizontal loads on the top surface. This research divides the asphalt layer interaction models into three categories: frictionless, simple friction model with friction coefficients, and full friction or full bond. The modelling uses the finite element method (FEM) with ABAQUS software, where the output results will provide strain data. Next, the strain data is checked against the limiting strain of NCAT to determine the dominant failure mode that occurs, whether it is fatigue cracking or rutting failure.

2. Material and methods

2.1. Finite Element Method

The finite element method is a numerical approach employed to address intricate engineering challenges by dividing structures into smaller, more manageable components. The theory behind FEM involves formulating mathematical models that represent physical phenomena, applying boundary conditions, and using variational methods to derive equations governing the behavior of each element. This approach allows for the analysis of various applications in mechanical, civil, and electrical engineering, providing insights into stress, strain, and other critical factors in design and analysis [13]. In flexible pavement theory, the FEM models the interaction between tyres and pavement as a two-dimensional axisymmetric problem. This method helps analyze factors like tyre pressure, loading conditions, and the material properties of pavement layers [14]. Figure 1 illustrates the three-dimensional (3D) model of the flexible pavement, which was analyzed using the finite element software ABAQUS.

The FE modeling uses a domain size where the boundary analysis is set at 40 times the area of the loading radius for the vertical boundary and 12 times the area of the loading radius for the horizontal boundary [15,16]. Since the rectangular contact radius used is equivalent to a radius of 150 mm in circular contact, the vertical boundary is set at 6 meters and the horizontal boundary is set at 1.8 meters from the center point of the radius. For the horizontal direction, this study adopts a domain size using a model size of 3.6 meters for both the transverse and longitudinal directions (1.8 meters from the center of the loading).

The selection of a large domain is critical for simulating a half-space. It is acknowledged, however, that absolute surface deflection in FE models is highly sensitive to the placement of the bottom boundary. As indicated by previous studies [17,18], deflection values increase with model depth and may not fully converge to a stable value even beyond 40R. Nevertheless, the primary objective of this study is not to predict exact in situ deflection values, but to conduct a comparative analysis of the effects of interlayer bonding and horizontal loading. For such purposes, the chosen conservative domain size is considered sufficient. It provides a consistent basis for analysis and ensures that the calculated differences in pavement response – particularly the critical strains, which are key to pavement durability – are attributable to the parametric variations being studied, rather than artifacts from the model boundaries.

For the boundary conditions, it is assumed that there is no displacement in the x and y axes on the longitudinal and transverse sides, respectively, on all four sides. At the bottom of the model, there is no movement in any direction (x, y, or z), meaning the subgrade stays vertically and horizontally [19]. A twenty-node quadratic brick element with reduced integration (C3D20R) is used with a fine mesh size in the loading area, while a coarse mesh size is applied elsewhere [3,20]. This should optimize modelling accuracy and improve the rate of convergence [21]. A mesh convergence test is conducted to determine accuracy [22,23]. The results of the convergence test, as shown in Fig. 2, indicate that as the number of elements increases, the resulting maximum von Mises stress value becomes more stable and the model's accuracy is sufficient for conducting numerical analysis.

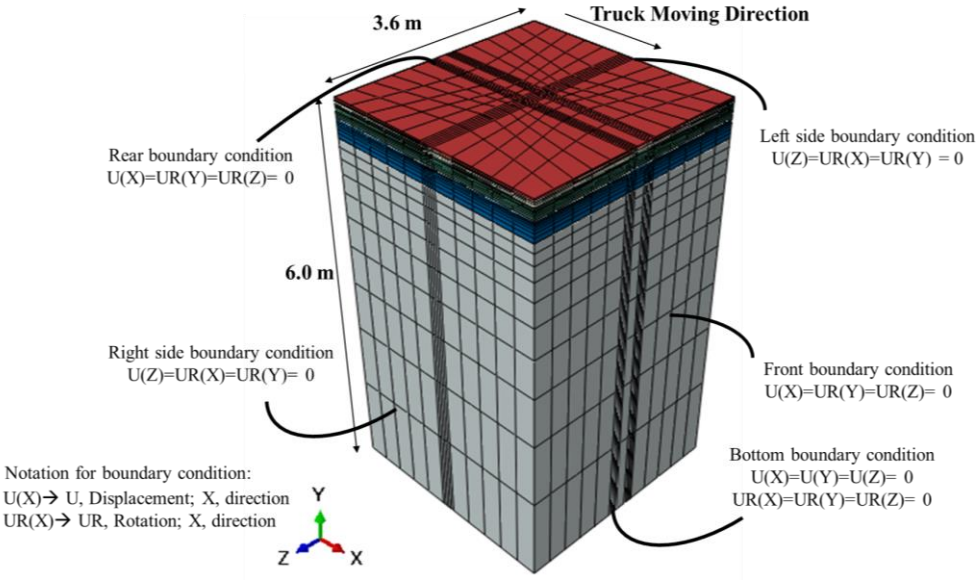

Fig. 1. 3D Model of flexible pavement. Source: own study

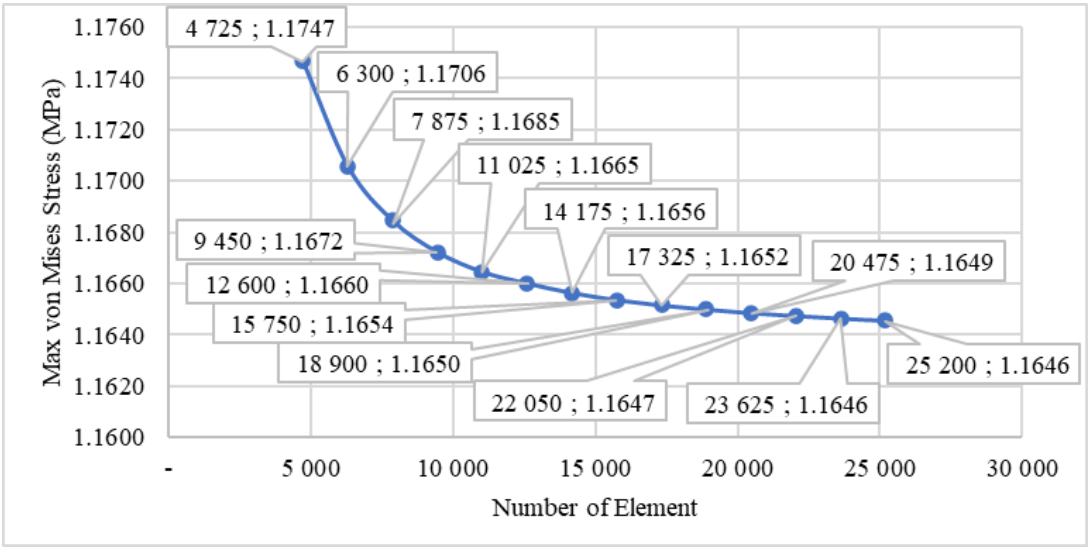

Fig. 2. Convergence test on FE model. Source: own study

2.2. Contact area and loading condition

To assess vehicle loads, it is essential first to define the configuration and axle loads to be applied to determine the contact area [1]. This research employs a standard axle load characterized by a single axle with dual tires (SADT), exerting a load of 80 kN on the pavement, with a spacing of 330 mm between the tires [24]. The most accurate representation of the contact area is a combination of a rectangle and two semicircles, as outlined in the Portland Cement Association method [6]. However, the shapes of the rectangle and semicircles for each tire can be changed into an equivalent rectangular area [1]. Figure 3 shows the shape and size of this equivalent rectangular area.

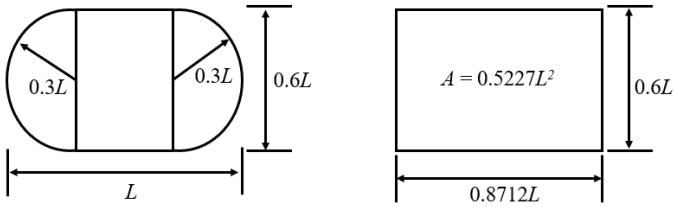

Fig. 3. Tire contact dimension. Source: [6]

Next, a rectangular contact area is used according to the Portland Cement Association (PCA) method based on the finite element procedure, with a length of 0.8172L and a width of 0.6L, where L represents the length of the tire and Ac denotes the contact area, which can be calculated using the following equation [6]

$$L = \frac{\sqrt{A_c}}{\sqrt{0{,}5227}} \quad (1)$$

$$A_c = \frac{load\ on\ each\ tire}{tire\ pressure} \quad (2)$$

Table 1 presents the outcomes of the calculations for the tire contact area and axle loads according to the Austroads standards. In the modeling and analysis using ABAQUS, this study employs a general static model as the loading condition. The static loading is represented by applying a contact pressure or vertical load of 0.551 MPa, which is uniformly distributed over the contact area and remains constant.

Horizontal loads on flexible pavement are a critical aspect overlooked mainly in traditional pavement design methodologies, which typically focus on vertical loads. Horizontal forces, such as those generated by vehicle acceleration, deceleration, and turning, significantly affect flexible pavements' structural integrity and performance. Research indicates that these forces can increase tensile strains at the surface and within the pavement layers, contributing to surface-initiated cracking and deformation, particularly in areas of frequent braking or turning, such as toll gates and airport runways. Both horizontal and vertical loads in the design of flexible pavements are highly recommended for road pavement design to avoid significant errors in the mechanistic pavement design stress-strain computation model when predicting pavement lifespan [8,25]. A horizontal load is also applied through the surface traction module. The value of the horizontal load is equal to half of the vertical load [8]. Figure 4 illustrates the modeling of both vertical and horizontal loads applied to the designated loading area in the ABAQUS software.

Table 1. Contact and load calculation. Source: own study

Parameter	Value
Configuration	Single Axle with Dual Tire (SADT)
Number of Wheels per axle	4
Axle Weight (kN)	80
Load on each tire, (kN)	80:4 = 20
80 psi tire pressure, (N/mm^2)	0.551
Estimated contact area, mm^2	4.500 lb/80 psi= 56.25 in = 36.290.25 mm^2
Length of tire imprint (rectangle-semicircle form), (mm)	$\frac{\sqrt{56.25}}{\sqrt{0.5227}}$=10.37 in= 263.49 mm
Length of equivalent area, 0,8712 L (mm)	230
Width of equivalent area, 0,6L (mm)	158
Measured tire contact area, Ac (mm^2)	230 x 158 = 36.340
Vertical Load / Contact Pressure (MPa)	20x10^3 : 36.340 = 0.551
Horizontal Load (MPa)	0.5 x 0.551= 0.275

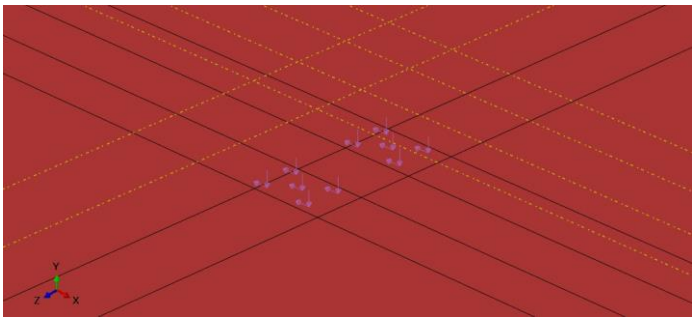

Fig. 4. Vertical and horizontal loads applied in ABAQUS. Source: own study

2.3. Input parameter and case model

To evaluate the effects of the layer interaction model and horizontal load, a flexible pavement is considered, which includes a 50 mm surface layer, an 80 mm binder layer, a 150 mm base layer, a 300 mm subbase layer, and a 5,420 mm thick subgrade layer. The material properties of this pavement are listed in Table 2, which includes elastic parameters like the modulus of elasticity, Poisson's ratio, and density.

Table 2. Material properties. Source: [3,26,27]

Material	Parameter	Value	Unit	Reference
Surface Course (SC)	Modulus of Elasticity, *E*	2.689	MPa	[27]
	Poisson Ratio	0.35		[27]
	Density	2.380	kg/m^3	[26]
Binder Course (BC)	Modulus of Elasticity, *E*	2.206	MPa	[27]
	Poisson Ratio	0.35		[27]
	Density	2.448	kg/m^3	[26]
Base (BSC)	Modulus of Elasticity, *E*	1.655	MPa	[27]
	Poisson Ratio	0.35		[27]
	Density	2.400	kg/m^3	[26]
Subbase (SB)	Modulus of Elasticity, *E*	110	MPa	[27]
	Poisson Ratio	0.4		[8]
	Density	2.040	kg/m^3	[26]
Subgrade (SG)	Modulus of Elasticity, *E*	50	MPa	[3]
	Poisson Ratio	0.45		[3]
	Density	1.600	kg/m^3	[3]

*) Assumed material Temperature: SC 55 °C; BC 49 °C; BSC 45°C [27]

To determine the effect of layer interaction with the simple friction model, the study uses 10 case models, of which 5 apply only vertical force and variations in interaction occurring at the Surface-Binder Interface. The other 5 cases implement a combination of loading, namely vertical and horizontal forces, with the same interaction variations as before. In these interaction variations, two extreme interaction conditions are also added: frictionless and full bond. The interaction relationship between the Base-Subbase and Subbase-Subgrade is modeled with tied conditions because of their high resistance to movement [8]. Table 3 below presents the cases and schemes used.

Table 3. Model case. *Source:* own study

Case	Horizontal load	SC-BC Interface	BC-BSC Interface	BSC-SB & SB-SG Interface
A	No	Frictionless	Frictionless	Frictionless
B	No	*Mu*=0.5	Tied	Tied
C	No	*Mu*=0.7	Tied	Tied
D	No	*Mu*=1	Tied	Tied
E	No	Tied	Tied	Tied
F	Yes	Frictionless	Frictionless	Frictionless
G	Yes	*Mu*=0.5	Tied	Tied
H	Yes	*Mu*=0.7	Tied	Tied
I	Yes	*Mu*=1	Tied	Tied
J	Yes	Tied	Tied	Tied

Mu = Friction Coefficient

2.4. Fatigue cracking and rutting life assessment

To assess fatigue cracking and rutting life, performance criteria developed by NCAT are used. These criteria recommend a limiting vertical compressive strain of 200 με on the subgrade and establish a limiting cumulative distribution for horizontal tensile strain in the asphalt layer (with key thresholds at 100 με for the 50th percentile and 326 με for the 99th percentile) [28]. The NCAT criteria are considered highly reliable as they were derived from extensive, full-scale accelerated pavement testing and validated against the field performance of numerous pavement sections, providing a robust link between predicted mechanistic responses and actual pavement distress.

3. Results

3.1. Effect of interaction interface model

Figure 5 presents an illustration of the results obtained from the finite element analysis, showing an example for the frictionless, simple friction, and full bond interaction case. The deflection bowl graph in Fig. 6 (also its maximum displacement value of each case in Fig. 7) shows the vertical displacement (U2) in the longitudinal direction plotted at the exact centerline of the wheel load, where three prominent variations in displacement values are observed among the 10 cases. The first, with the maximum deflection value, corresponds to Case A and F, which model frictionless interaction across all layers. The frictionless condition is a modelling interaction or contact assumption that the surfaces in contact do not resist sliding against each other [29]. In a contact scenario without friction (frictionless), the continuity of shear stress and radial displacement is substituted with zero shear stress on both sides of the interface [6]. The absence of shear forces allows for a more efficient redistribution of loads across the layers, contributing to a more significant deflection in the upper layer.

In the medium deflection range, which includes Cases B, C, D, G, H, and I, these six cases apply simple friction contact with input values for the coefficient of friction. In this frictional condition, the contacting surfaces transmit shear and normal forces between them [29]. The presence of shear forces can still limit the movement between layers, allowing the load distribution to cause concentration in specific layers and potentially reduce the deflection values, although not as tightly as in the full bond model. Figure 7 shows that the deflection value decreases as the friction coefficient increases.

A tie constraint is implemented in the condition of minimum deflection value, which corresponds to Cases E and J, which apply the full bond condition. A tie constraint binds two separate surfaces together so they have no relative motion. This type of constraint allows you to fuse two regions [29]. In the full bond model, the absence of relative movement, because all layers are bound to each other, can lead to load concentration in specific layers and reduce deflection in the upper layer.

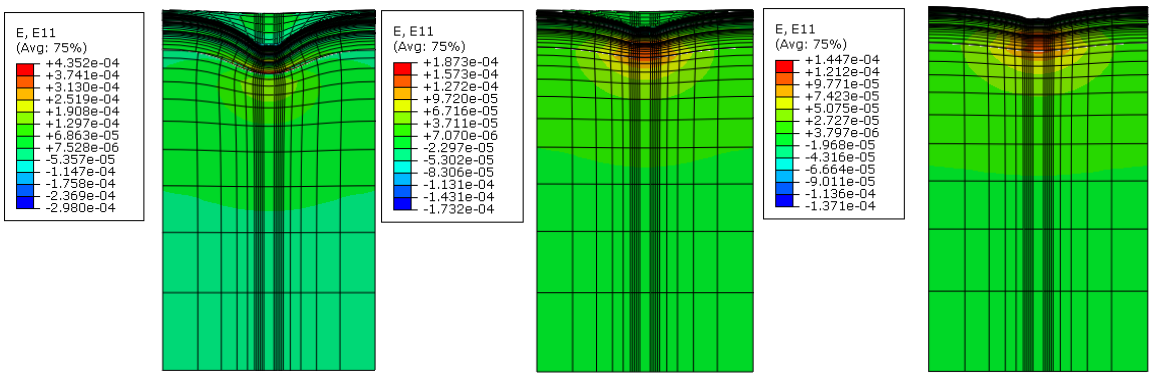

(a) frictionless (b) simple friction (c) fullbond

Fig. 5. ABAQUS result visualization

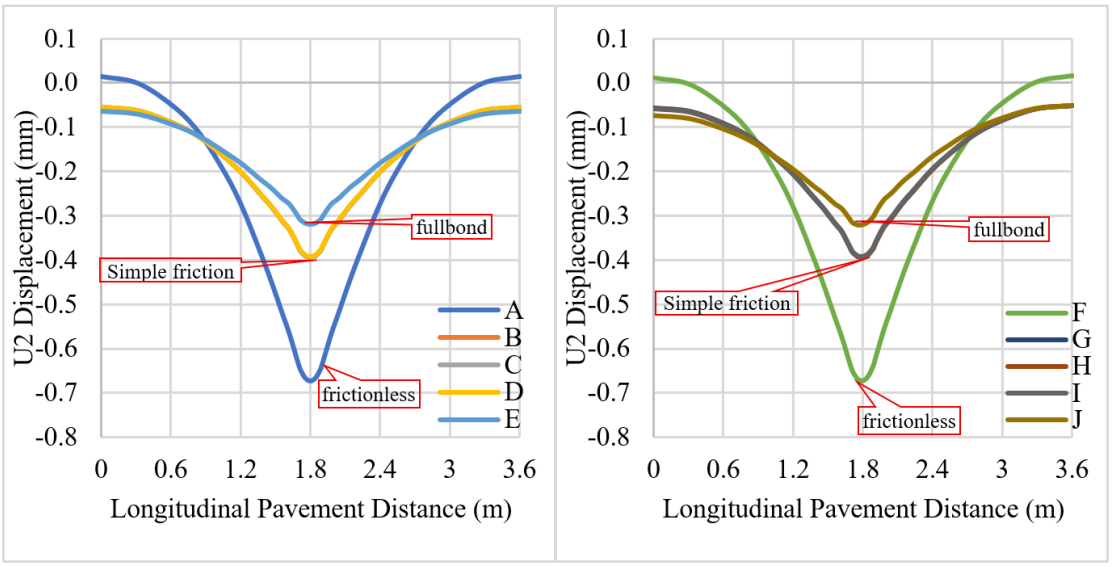

(a) vertical load applied (b) vertical and horizontal loads applied

Fig. 6. U2 displacement in longitudinal direction at top of surface course layer. Source: own study

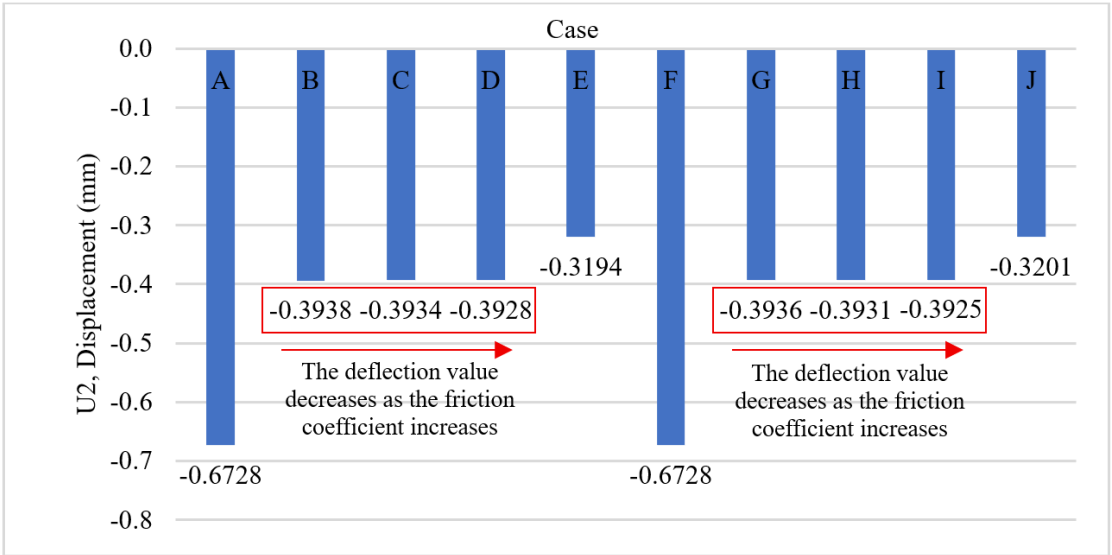

Fig. 7. Max U2 displacement value at top of surface course layer. Source: own study

Following this, the effect of layer interaction on the pavement's structural response will be discussed, focusing on the horizontal tensile strain beneath the bituminous layer and the vertical compressive strain at the surface of the subgrade layer. These factors are typically used in the mechanistic-empirical design approach for flexible pavements to assess pavement lifespan [8,24,30,31].

Figure 8 presents the charts illustrating the horizontal strain in the driving direction (E11) at the base of the binder course. These graphs are separated to distinguish the effects of horizontal force, where Cases A, B, C, D, and E do not apply horizontal force, while Cases F, G, H, I, and J do apply horizontal force. The output shows the maximum strain, specifically the horizontal tensile strain, which aligns with the assumptions of the mechanistic-empirical modeling. Next, as shown in Figure 8, there are three variations of strain values, namely the cases that apply frictionless contact, contact with friction coefficients, and full bond contact. The horizontal tensile strain with the highest value occurs in the frictionless contact mode, followed by full bond and simple friction.

In the case of strain values, the full bond shows greater values compared to simple friction. Previous research also indicated that the horizontal strain in full bond is greater than that in simple friction, with values of 200 microstrain and a range of 75-100 microstrain [8]. Of course, these values differ from those in this study because of differences in material properties and structural thickness. Figure 9 shows a summary of the maximum horizontal strain values (E11) for all cases, and indicates that the horizontal tensile strain value decreases as the friction coefficient increases.

The charts presented in Fig. 10 illustrate the results of vertical compressive strain at the surface of the subgrade. The highest vertical compressive strain occurs under the simple friction interaction model, followed by fullbond and the frictionless condition, as seen in Fig. 10. In the simple coefficient of friction model condition, where the compressive strain is greater than the full bond model, this finding is also consistent with results from previous studies [8,32].

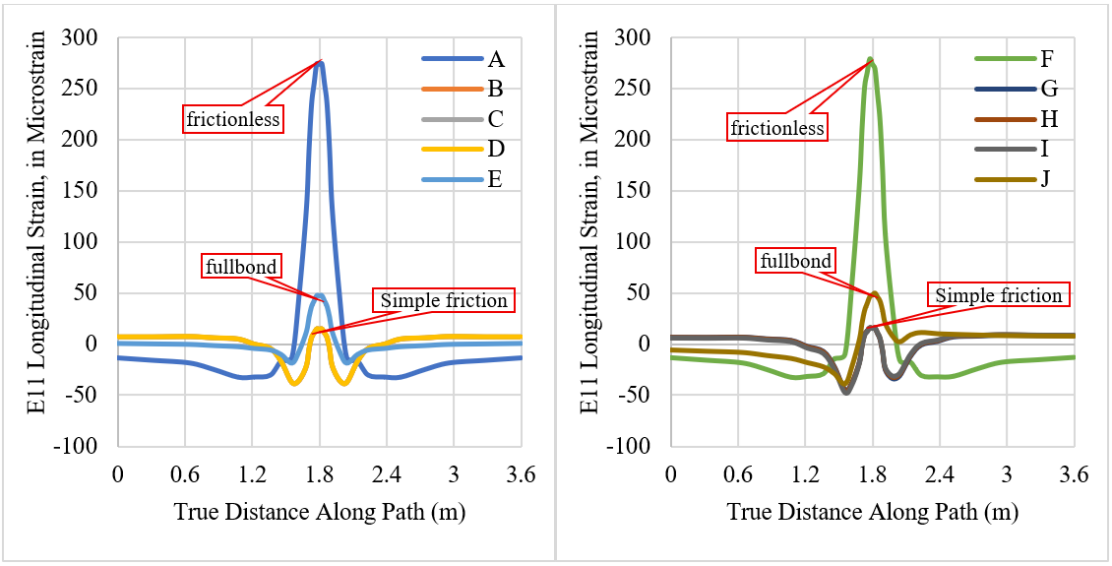

(a) vertical load applied (b) vertical and horizontal loads applied

Fig. 8. E11 horizontal strain beneath binder course layer. Source: own study

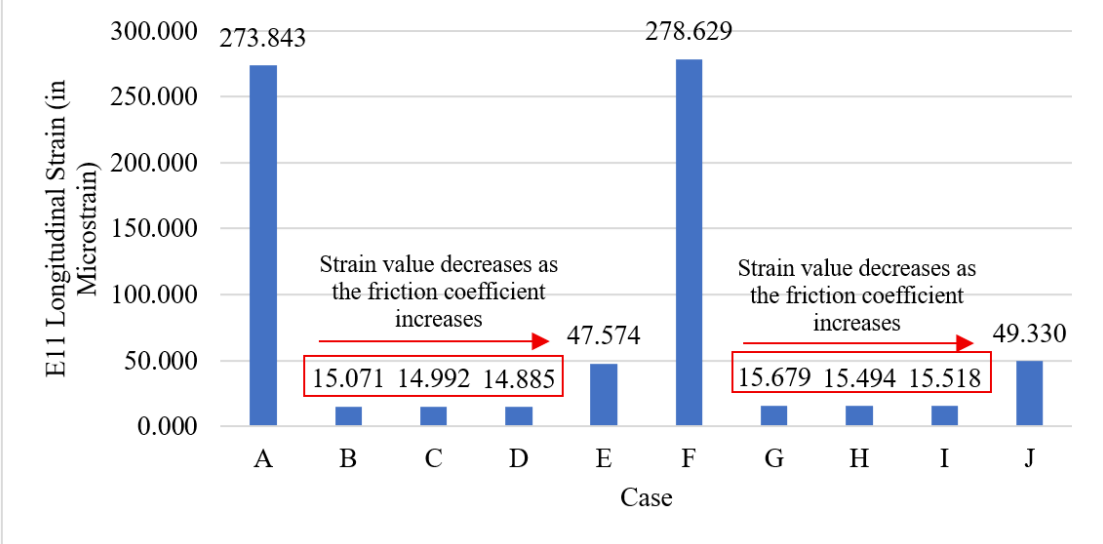

Fig. 9. Max E11 strain value at binder course layer. Source: own study

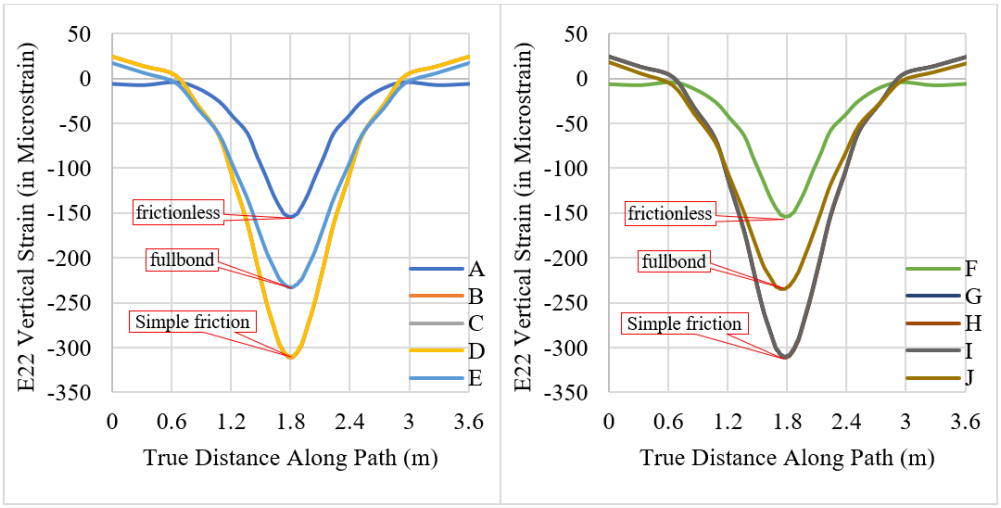

(a) vertical load applied (b) vertical and horizontal loads applied

Fig. 10. E22 vertical strain in longitudinal direction at top of subgrade layer. Source: own study

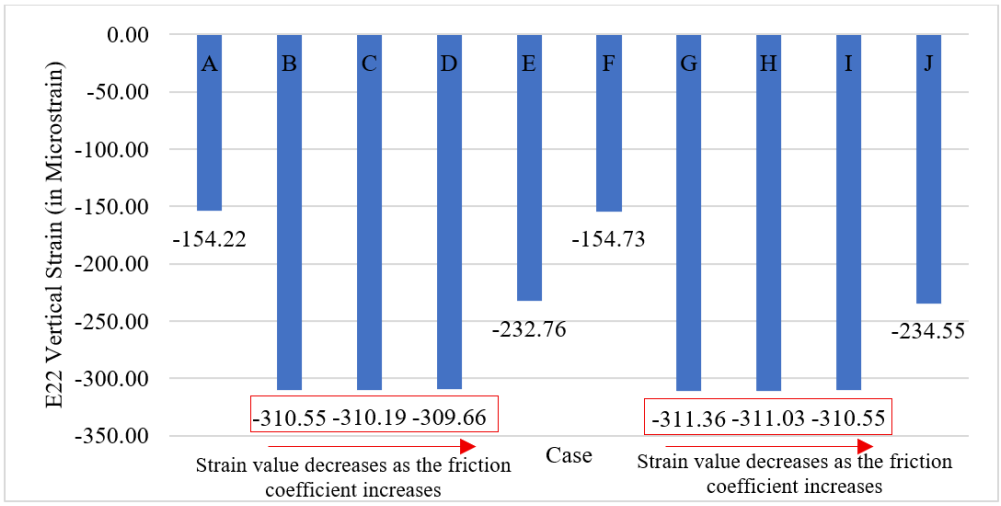

Fig. 11. Max E22 strain at top of subgrade layer. Source: own study

3.2. Effect of horizontal load

Table 4 shows the maximum horizontal tensile strain values in the asphalt layer and maximum vertical compression strain values in the non-bituminous layer that simultaneously apply horizontal and vertical loads. A direct comparison is made between the cases. From the table, for the overall case there is a significant increase in horizontal strain values, particularly at the top and underlying the surface course and for the top of the binder course layer, particularly for the full-bond interaction model. This increase can trigger the onset of cracking in the asphalt surface layer, which contrasts with the previous traditional assumption that cracking begins from the bottom of the asphalt [32]. In contrast, for the non-bituminous layer, the effect of the horizontal load on the strain value is not significant [8,33].

As shown in Figure 7 and Table 5, the application of horizontal loads has no significant effect on the vertical displacement (U2) at the top surface, indicating a minor impact on the weight and shape of the surface displacement bowls [8]. However, Figure 12 illustrates the variations in the shape of the horizontal strain curves at the upper surface, highlighting a shift from compressive strain to tensile strain near the center of the tire contact area [34,35,36].

Table 4. Value of max horizontal tensile strain (bituminous layer) and max vertical compression strain (nonbituminous layer) with and without horizontal load. Source: own study

Location	Value	Strain (in microstrain)										Change (%)				
		No Horizontal Load					With Horizontal Load									
		A	B	C	D	E	F	G	H	I	J	AvF	BvG	CvH	DvI	EvJ
Top SC	Max	17.17	14.43	14.44	14.46	21.56	184.03	229.11	226.42	222.89	128.54	971.54	1487.95	1467.71	1441.69	496.27
Bottom SC	Max	221.25	155.67	154.85	153.62	12.96	294.90	219.48	214.69	208.43	27.50	33.29	40.99	38.64	35.68	112.18
Top BC	Max	28.00	26.04	26.01	25.96	12.96	28.47	27.78	28.25	28.86	27.56	1.68	6.68	8.62	11.16	112.64
Bottom BC	Max	273.84	15.07	14.99	14.88	47.57	278.63	15.68	15.49	15.52	49.33	1.75	4.03	3.35	4.25	3.69
Top BSC	Min	9.16	152.08	151.49	150.64	137.25	9.37	155.51	154.96	154.13	140.65	2.30	2.26	2.29	2.32	2.48
Bottom BSC	Min	322.87	180.66	180.29	179.75	139.04	326.08	182.45	182.13	181.66	141.46	0.99	0.99	1.02	1.06	1.74
Top SB	Min	64.31	398.91	398.08	396.88	296.55	64.45	402.37	401.66	400.59	301.58	0.21	0.87	0.90	0.93	1.70
Bottom SB	Min	656.65	251.19	250.90	250.48	188.41	658.97	251.84	251.58	251.19	189.92	0.35	0.26	0.27	0.28	0.80
Top SG	Min	154.22	310.55	310.19	309.66	232.76	154.73	311.36	311.03	310.55	234.55	0.33	0.26	0.27	0.29	0.77

Table 5. U2 max displacement result of horizontal load effect at top of surface course. Source: own study

Case	No Horizontal Load	With Horizontal Load	Change
A vs F	-0.67277	-0.67277	0.00%
B vs G	-0.39375	-0.39357	0.05%
C vs H	-0.39337	-0.39312	0.06%
D vs I	-0.39282	-0.39249	0.08%
E vs J	-0.31937	-0.32009	0.23%

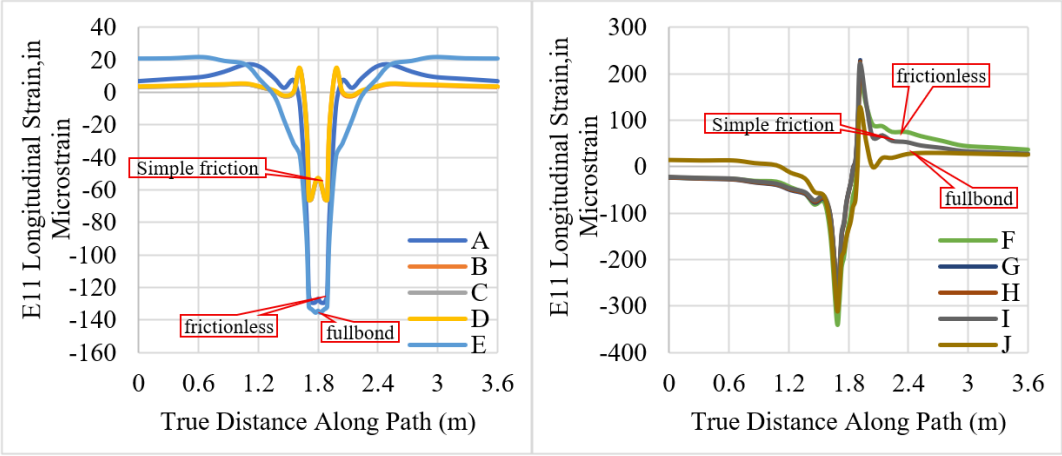

(a) vertical load applied (b) vertical and horizontal loads applied

Fig. 12. E11 horizontal strain in longitudinal direction at top of surface course layer. Source: own study

3.3. Effect of interaction model and horizontal load in critical strain

Table 6 shows the results of critical strain data for fatigue cracking and rutting assessment of each modeled pavement. The fatigue cracking related strain value is taken from the maximum horizontal tensile strain value across several locations in the bitumen layer, while the rutting value is taken from the maximum vertical compression strain value from the surface of the subgrade layer. To assess the potential for fatigue cracking and rutting, this study uses the performance criteria developed by the National Center for Asphalt Technology (NCAT). These criteria recommend a limiting vertical compressive strain of 200 με at the top of the subgrade to prevent rutting and establish a limiting cumulative distribution for horizontal tensile strain in the asphalt layer (with key thresholds at 100 με for the 50th percentile and 326 με for the 99th percentile) to control fatigue cracking [28]. Based on these criteria, the results in Table 6 indicate that rutting at the top of the subgrade (Top SG) is the dominant failure mode in nearly all analyzed scenarios. This suggests that the long-term performance of this pavement structure is primarily controlled by the subgrade's resistance to permanent deformation.

Fatigue Cracking Analysis

For fatigue cracking analysis, although results varied between cases, it is noteworthy that all calculated strain values (maximum of 295 με in Case F) remained below the critical 99th percentile NCAT threshold of 326 με. This indicates that the asphalt layer design possesses very high reliability against fatigue cracking for all conditions tested. The primary trends observed are the effect of interlayer bonding and the effect of horizontal loading. For the effect of interlayer bonding, improving the bond quality significantly reduces tensile strain. The most drastic reduction occurs in the fully bonded condition (Case E: 48 με), which demonstrates that a monolithic pavement structure is highly effective at suppressing tensile strain. Second, the application of a horizontal load consistently increases tensile strain across all bonding levels. This significant increase (e.g., from 48 με to 129 με in the full-bond case) confirms that horizontal loading is a critical factor that can accelerate the initiation of fatigue cracking.

Table 6. Result of pavement critical strain under limiting strain

Case	Fatigue Cracking			Rutting			Critical Location
	Max. Strain	Limiting Strain	Result	Max. Strain	Limiting Strain	Result	
A	274	100 με for the 50th percentile and 326 με for the 99th percentile	Meet	154	200 με	Meet	Top SG
B	156		Meet	311		Fail	Top SG
C	155		Meet	310		Fail	Top SG
D	154		Meet	310		Fail	Top SG
E	48		Meet	233		Fail	Top SG
F	295		Meet	155		Meet	Bottom SC
G	229		Meet	311		Fail	Top SG
H	226		Meet	311		Fail	Top SG
I	223		Meet	311		Fail	Top SG
J	129		Meet	235		Fail	Top SG

Rutting Analysis

The rutting analysis, governed by the vertical compressive strain at the top of the subgrade, reveals more critical results. The majority of cases fail to meet the 200 με NCAT threshold, indicating that the pavement would not qualify as a perpetual pavement under these conditions. From the effect of interlayer bonding, an interesting phenomenon was discovered where the frictionless case (Case A) yielded the lowest compressive strain (154 με) and met the NCAT criterion. Conversely, when friction was introduced (Cases B/C/D), the compressive strain surged to ~310 με. This suggests that a frictional interface transfers vertical loads more directly to the subgrade, thereby significantly increasing rutting potential compared to a no-bond condition. For the effect of horizontal loading, in contrast to its impact on fatigue cracking, the application of a horizontal load has a negligible effect on the compressive strain at the top of the subgrade. This confirms that horizontal shear forces are primarily resisted by the stiffer upper layers, and their influence on vertical stresses deep in the subgrade is minimal. Also, this is because horizontal loads mainly influence the horizontal strains in the bituminous layers and, to a lesser extent, the vertical strains at the top of the subgrade [8,33].

Critical Location and dominant failure mode

Among all scenarios, Case F (frictionless with horizontal load) is the only instance where the critical location is determined by fatigue cracking potential at the bottom of the surface course (Bottom SC). This occurs because in this case, the compressive strain on the subgrade (155 με) still meets the NCAT criterion, while the tensile strain in the asphalt (295 με) becomes relatively more critical due to the horizontal load. However, for all other, more realistic cases where interlayer bonding exists (friction or full bond), the failure mode that governs the pavement's service life is rutting at the top of the subgrade (Top SG), which consistently exceeds the limit established by NCAT.

4. Conclusion

This study investigated the influence of interlayer bonding conditions and horizontal loading on the mechanistic response of flexible pavements, with performance benchmarked against NCAT criteria. The analysis reveals several key findings:

a. Subgrade rutting was identified as the dominant failure mode. In most realistic (bonded) scenarios, the vertical compressive strain at the top of the subgrade exceeded the 200 με perpetual pavement threshold, indicating that subgrade performance is the primary factor controlling the pavement's service life.
b. Horizontal loads and interlayer bonding have distinct and critical effects on different failure modes.
   – Horizontal loading critically increases the horizontal tensile strain at the bottom of the asphalt layer (accelerating fatigue damage) but has a negligible effect on the vertical compressive strain at the top of the subgrade (rutting).
   – Improved interlayer bonding is highly effective at reducing fatigue strain. However, it can paradoxically increase rutting potential by transferring vertical stress more directly to the subgrade compared to a frictionless condition.

These findings underscore the importance of including horizontal loads in fatigue analysis and selecting an appropriate interface model for rutting analysis. While the full bond and frictionless cases define the theoretical performance boundaries, the simple friction model offers a more realistic representation for design. Finally, field and laboratory testing are recommended to calibrate practical friction coefficients, further enhancing the accuracy of future pavement models.

Funding

This work was not supported by any external funding.

References

[1] Z. M. Aljaleel, N. Yasoub, Y. K. H. Atemimi, “Finite Element Modeling for Flexible Pavement Behavior under Repeated Axle Load”, *Engineering, Technology and Applied Science Research* 14(4), (2024) 15180–15186. https://doi.org/10.48084/etasr.7505

[2] P. Praveen Kumar, B. V. Kiran Kumar, S. Manjunatha, K. G. Subramanya, “Finite Element Modeling by ABAQUS for Rutting in Flexible Pavement”, *Civil Engineering and Architecture*, 12(3), (2024) 1576–1584. https://doi.org/10.13189/cea.2024.120323

[3] A. Nega, D. Gedafa, H. Nikraz, “Stress and Strain Characteristics in Flexible Pavement Using Three-Dimensional Nonlinear Finite Element Analysis”, *International Journal of Pavement Research and Technology* 17 (2024) 1498–1512. https://doi.org/10.1007/s42947-024-00422-2

[4] M. K. Charyulu, J. B. Sheeler, “Theoretical Stress Distribution Elastic Multi-Layered System”, 1968. Accessed: Feb. 08, 2025. [Online]. Available: http://onlinepubs.trb.org/Onlinepubs/hrr/1968/228/228-002.pdf

[5] E. S. Hariyadi, K. P. Aurum, B. S. Subagio C, “Theoretical Study of Bonding Condition at the Interface between Asphalt Pavement Layers”, *Journal of the Eastern Asia Society for Transportation Studies* 10 (2013) 1590–1597. https://doi.org/10.11175/easts.10.1590

[6] Y. H. Huang, *Pavement Analysis and Design (Second Edition)*. Prentice Hall ; Pearson Education, 2009.

[7] J. Uzan, “Influence of the Interface Condition on Stress Distribution in a Layered System”, 1976. Accessed: Feb. 08, 2025. [Online]. Available: https://onlinepubs.trb.org/Onlinepubs/trr/1976/616/616-015.pdf

[8] S. A. Romanoschi, “Characterization of Pavement Layer Interfaces”, Louisiana State University and Agricultural and Mechanical College, 1999. https://doi.org/10.31390/gradschool_disstheses.7008

[9] D. L. De Jong, M. G. F. Peatz, *Computer Program, Layered System Under Normal and Tangential Surface Loads: BISAR (bitumen Structures Analysis in Roads): Users Manual (abbreviated Version)*. Koninklijke Shell Laboratorium (Amsterdam, Netherlands), 1972.

[10] N. H. Zulkifili, M. H. Sutanto, “The Influence of Bonding between Layers on Pavement Performance, a Case Study of Malaysian Road”, in *E3S Web of Conferences*, EDP Sciences, Nov. 2018. https://doi.org/10.1051/e3sconf/20186509002

[11] N. L. Nguyen, V. D. Dao, M. L. Nguyen, D. H. Pham, “Investigation of Bond Between Asphalt Layers in Flexible Pavement”, Springer, Dordrecht, 2016, 519–525. https://doi.org/10.1007/978-94-024-0867-6_73

[12] S. S. Sayyed, R. P. Patil, A. B. Tapase, A. C. Attar, P. G. Chandak, “Review and Assessment of Flexible Pavement”, Springer, Cham, 2018, 139–149. https://doi.org/10.1007/978-3-319-96241-2_12

[13] S. Musa, *Finite Element Analysis*. De Gruyter, 2023. https://doi.org/10.1515/9781683924173

[14] A. B. Tapase, M. S. Ranadive, “Predicting Performance of Flexible Pavement Using Finite Element Method”, Springer, Cham, 2017, 137–146. https://doi.org/10.1007/978-3-319-61908-8_11

[15] J. M. Duncan, C. L. Monismith, E. L. Wilson, “Finite Element Analyses of Pavements”, *47th AnnuaI Meeting of Committee Mechanics of Earth Masses and Layered Systems*, 1968, Accessed:

Feb. 08, 2025. [Online]. Available: https://onlinepubs.trb.org/Onlinepubs/hrr/1968/228/228-003.pdf

[16] M. Koohmishi, "Comparison of Pavement Layers Responses with Considering Different Models for Asphalt Concrete Viscoelastic Properties", *Slovak Journal of Civil Engineering* 21(2), (2013) 15–20. https://doi.org/10.2478/sjce-2013-0008

[17] R. Nagórski, P. Tutka, M. Złotowska, "Defining the domain and boundary conditions for finite element model of flexible road pavement", *Roads and Bridges - Drogi i Mosty* 16(4), (2017) 265–277. https://doi.org/10.7409/rabdim.017.017

[18] M. Nagórska, "On a certain method of selection of domain for finite element modelling of the layered elastic half-space in the static analysis of flexible pavement", *Archives of Civil Engineering* 58(4) (2012) 477–501. https://doi.org/10.2478/v.10169-012-0026-8

[19] O. C. Assogba, Y. Tan, X. Zhou, C. Zhang, J. N. Anato, "Numerical investigation of the mechanical response of semi-rigid base asphalt pavement under traffic load and nonlinear temperature gradient effect", *Construction and Building Materials* 235 (2020) 1–25. https://doi.org/10.1016/j.conbuildmat.2019.117406

[20] S. Li, "Numerical investigation on viscoelastic response of asphalt mixture under tire braking slip", *Case Studies in Construction Materials* 18 (2023) e02009. https://doi.org/10.1016/j.cscm.2023.e02009

[21] M. A. Elseifi, I. L. Al-Qadi, P. J. Yoo, "Viscoelastic Modeling and Field Validation of Flexible Pavements", *Journal of Engineering Mechanics* 132(2) (2006) 172–178. https://doi.org/10.1061/(ASCE)0733-9399(2006)132:2(172)

[22] A. Mahfuda, S. Siswosukarto, B. Suhendro, "The Influence of Temperature Variations on Rigid Pavement Concrete Slabs", *Journal of the Civil Engineering Forum* 9(2) (2023) 139–150. https://doi.org/10.22146/jcef.5744

[23] M. M. Rahman, S. Saha, A. S. A. Hamdi, M. J. Bin Alam, "Development of 3-D Finite Element Models for Geo-Jute Reinforced Flexible Pavement", *Civil Engineering Journal (Iran)* 5(2) (2019) 437–446. https://doi.org/10.28991/cej-2019-03091258

[24] M. Moffatt, A. Papacostas, "Guide to Pavement Technology Part 2: Pavement Structural Design", Sydney, Apr. 2024. Accessed: Feb. 08, 2025. [Online]. Available: https://austroads.gov.au/publications/pavement/agpt02/media/AGPT02-24_Guide_to_Pavement_Technology_Part_2_Pavement_Structural_Design.pdf

[25] E. S. Barber, "Shear loads on pavements", *First International Conference on the Structural Design of Asphalt Pavements*, 1062, 354–357, Accessed: Feb. 08, 2025. [Online]. Available: https://trid.trb.org/View/717088

[26] P. Liu, D. Wang, J. Hu, M. Oeser, "SAFEM - Software with graphical user interface for fast and accurate finite element analysis of asphalt pavements", *Journal of Testing and Evaluation* 45(4) (2016) 1301–1315. https://doi.org/10.1520/JTE20150456

[27] A. H. Abed, A. A. Al-Azzawi, "Evaluation of Rutting Depth in Flexible Pavements by Using Finite Element Analysis and Local Empirical Model", *American Journal of Engineering and Applied Sciences* 5(2) (2012) 163–169. https://doi.org/10.3844/ajeassp.2012.163.169

[28] N. Tran, M. M. Robbins, D. H. Timm, J. R. Willis, C. Rodezno, "Refined Limiting Strain Criteria And Approximate Ranges Of Maximum Thicknesses For Designing Long-Life Asphalt Pavements (First Revision)", 2016.

[29] Dassault Systèmes, "ABAQUS Version 6.14 Documentation", 2014. Accessed: Feb. 08, 2025. [Online]. Available: http://62.108.178.35:2080/v6.14/index.html

[30] G. Engleng, "Strain Transfer Function in Flexible Pavements", *International Journal of Advance Research in Science and Engineering* 5(12) (2016) Accessed: Feb. 08, 2025. [Online]. Available: http://ijarse.com/images/fullpdf/1481516979_1450.pdf

[31] L. F. Walubita, M. F. C. van De Ven, "Stresses and Strains in Asphalt-Surfacing Pavement", *South African Transport Conference 'Action in Transport for the New Millennium' Conference Papers*, 2000, Accessed: Feb. 08, 2025. [Online]. Available: https://repository.up.ac.za/bitstream/handle/2263/8338/76%20Walubita.pdf

[32] S. A. Romanoschi, J. B. Metcalf, "Effects of Interface Condition and Horizontal Wheel Loads on the Life of Flexible Pavement Structures", *Transportation Research Record (Transportation Research Board of the National Academies)* 1778(1) (2001) 123-131. https://doi.org/10.3141/1778-15

[33] A. El-Desouky, G. El-Sheakhy, "New Concept for the Design of Flexible Pavement at Critical Highway Sections", *17th International Conference on Aerospace Sciences & Aviation Technology, Asat - 17*, 17–116, 2017. https://doi.org/10.21608/asat.2017.22747

[34] Z. Nian Mei, W. Xu Dong, "Deformation Analysis of Pavement Structures under Coexistence of Vertical and Horizontal Loads", *Applied Mechanics and Materials* 44–47 (2010) 3053–3059. https://doi.org/10.4028/www.scientific.net/AMM.44-47.3053

[35] C. S. Gideon, J. M. Krishnan, "Influence of Horizontal Traction on Top-Down Cracking in Asphalt Pavements", Springer, Dordrecht, 2012 1069–1079. https://doi.org/10.1007/978-94-007-4566-7_102

[36] J. Jiao, S. D. Meng, Q. Jiao, N. Li, "The Mechanical Response Analysis of the Airport Asphalt Pavement Considering Horizontal Load", *Advanced Materials Research* 645 (2013) 471–475. https://doi.org/10.4028/www.scientific.net/AMR.645.471